A full subtraction approach for finite element method based source analysis using constrained Delaunay tetrahedralisation

F. Drechsler, C.H. Wolters, T. Dierkes, H. Si, L. Grasedyck

PII: S1053-8119(09)00176-1
DOI: doi: 10.1016/j.neuroimage.2009.02.024
Reference: YNIMG 6014

To appear in: *NeuroImage*

Received date: 5 November 2008
Accepted date: 13 February 2009

Please cite this article as: Drechsler, F., Wolters, C.H., Dierkes, T., Si, H., Grasedyck, L., A full subtraction approach for finite element method based source analysis using constrained Delaunay tetrahedralisation, *NeuroImage* (2009), doi: 10.1016/j.neuroimage.2009.02.024

A full subtraction approach for finite element method based source analysis using constrained Delaunay tetrahedralisation.

F. Drechsler [a], C.H. Wolters [b,*], T. Dierkes [b], H. Si [c], L. Grasedyck [a]

[a] *Max-Planck-Institut für Mathematik in den Naturwissenschaften, Leipzig, Germany*

[b] *Westfälische Wilhelms-Universität Münster, Institut für Biomagnetismus und Biosignalanalyse, Malmedyweg 15, 48149 Münster, Germany*

[c] *Weierstraß-Institut für Angewandte Analysis und Stochastik, Berlin, Germany.*

Abstract

A mathematical dipole is widely used as a model for the primary current source in electroencephalography (EEG) source analysis. In the governing Poisson-type differential equation, the dipole leads to a singularity on the right-hand side, which has to be treated specifically. In this paper, we will present a full subtraction approach where the total potential is divided into a singularity and a correction potential. The singularity potential is due to a dipole in an infinite region of homogeneous conductivity. The correction potential is computed using the finite element (FE) method. Special care is taken in order to evaluate the right-hand side integral appropriately with the objective of achieving highest possible convergence order for linear basis functions. Our new approach allows the construction of transfer matrices for fast computation of the inverse problem for anisotropic volume conductors.

A constrained Delaunay tetrahedralisation (CDT) approach is used for the generation of high-quality FE meshes. We validate the new approach in a four-layer sphere model with a highly conductive cerebrospinal fluid (CSF) and an anisotropic skull compartment. For radial and tangential sources with eccentricities up to 1mm below the CSF compartment, we achieve a maximal relative error of 0.71% in a CDT-FE model with 360K nodes which is not locally refined around the source singularity and therefore useful for arbitrary dipole locations. The combination of the full subtraction approach with the high quality CDT meshes leads to accuracies that, to the best of the authors knowledge, have not yet been presented before.

Key words: electroencephalography, source reconstruction, finite element method, dipole, full subtraction approach, constrained Delaunay tetrahedralisation, validation in four-layer sphere models, cerebrospinal fluid, conductivity anisotropy, projected subtraction approach, transfer matrix

1 Introduction

Inverse methods are used to reconstruct current sources in the human brain by means of electroencephalography (EEG) or magnetoencephalography (MEG) measurements of, e.g., event related fields or epileptic seizures (Hämäläinen et al., 1993; Michel et al., 2004; Plummer et al., 2008; Rullmann et al., 2008). A critical component of the inverse neural source reconstruction is the solution of the forward problem, i.e., the simulation of the fields at the head surface for a known primary current source in the brain. Because of the avail-

* Corresponding author. PD.Dr.rer.nat. Carsten H.Wolters, Tel.: +49/(0)251/83-56904, Fax: +49/(0)251/83-56874

Email address: {carsten.wolters}@uni-muenster.de (C.H. Wolters).

ability of quasi-analytical EEG forward problem solution formulas (de Munck and Peters, 1993), the head volume conductor is still often represented by a multi-layer sphere model. However, this model is just a rough approximation to the reality, so that numerical approximation methods are more and more frequently used such as the boundary element method (BEM) (Hämäläinen et al., 1993; Kybic et al., 2005), the finite volume method (FVM) (Cook and Koles, 2006), the finite difference method (FDM) (Hallez et al., 2005) or the finite element method (FEM). This paper focuses on the FEM which allows high accuracy for the numerical solution of elliptic partial differential equations since it is specifically tailored to the corresponding variational formulation (Hackbusch, 1992; Braess, 2007; Dahmen and Reusken, 2008) and since it allows high flexibility in modelling the forward problem in geometrically complicated inhomogeneous and anisotropic head volume conductors (Bertrand et al., 1991; Awada et al., 1997; van den Broek, 1997; Marin et al., 1998; Schimpf et al., 2002; Zhang et al., 2006; Wolters et al., 2007a,b). Advantages of the FEM are that the underlying weak formulation of the boundary value problem and its Galerkin-discretisation allow on the one side an appropriate and accurate modelling of the physics and offers on the other side a mathematically clean treatment of cases with low regularity (Hackbusch, 1992; Braess, 2007; Dahmen and Reusken, 2008) like the one in EEG source analysis with the discontinuous tissue conductivities. As will be shown, the FEM discretisation can be adapted to the structure of the solution function by means of appropriate mesh refinements and coarsenings so that highest accuracy can be achieved with a reasonable number of nodes.

It was shown in (Sarvas, 1987; de Munck et al., 1988; Hämäläinen et al., 1993; Murakami and Okada, 2006) that the mathematical dipole is an adequate

model to represent the primary current which is caused by a synchronous activity of tens of thousands of densely packed apical dendrites of large pyramidal cells oriented in parallel in the human cortex. The dipole model is thus considered to be the "atomic" structure of the primary current density distribution that has to be reconstructed within the inverse problem. Hence, one of the key questions for all 3D forward modelling techniques is the appropriate modelling of the potential singularity introduced into the differential equation by means of the mathematical dipole.

Direct potential approaches (Yan et al., 1991; Buchner et al., 1997) approximate the dipole moment through optimally distributed monopolar sources and sinks on neighbouring FE nodes of the source location. This approach leads to finite distances between the poles that seem reasonable and it performs well in validation studies (Buchner et al., 1997; Wolters et al., 2007b). However, a disadvantage of direct approaches is the absence of a well-understood mathematical theory. Furthermore, in recent comparison studies of different direct methods with the subtraction approach (Awada et al., 1997; Schimpf et al., 2002), it is concluded that the overall best accuracy is achieved using the latter method.

A subtraction approach for the modelling of a mathematical dipole in FE-based source analysis was widely suggested (Bertrand et al., 1991; Awada et al., 1997; van den Broek, 1997; Marin et al., 1998; Schimpf et al., 2002; Wolters et al., 2007a). All proposed approaches have in common that the total potential is divided into an analytically known singularity potential and a singularity-free correction potential which can then be approximated numerically using an FE approach. The subtraction approach is applicable for arbitrary geometries and the FE discretisation allows for a treatment of

geometric details and tissue inhomogeneities and anisotropies. In (Wolters et al., 2007a), a theoretical insight was given into the subtraction approach. A proof was given for existence and uniqueness of a weak solution in the function space of zero-mean potential functions and convergence properties of the FE-approach to the correction potential were stated. A *projected subtraction method* was proposed where the singularity potential was projected in the FE space (Wolters et al., 2007a). This approach was shown to perform well in a three-compartment (skin, skull, brain) sphere model provided that the so-called *source eccentricity* was limited to 95%. The eccentricity is generally defined as the percent ratio of the distance between the source location and the model midpoint divided by the radius of the inner sphere. When considering a three-shell model, 95% eccentricity seems reasonable because the dipoles that are located in the cortex will have an eccentricity even lower than 92% as reported in (Marin et al., 1998).

However, the three-compartment model of the head, which is still most often used in source analysis (see, e.g., (Hämäläinen et al., 1993; Michel et al., 2004; Kybic et al., 2005; Wolters et al., 2007a)), ignores the cerebrospinal fluid (CSF) compartment between the cortex and the skull. (Baumann et al., 1997) showed for a group of 7 human subjects (neurosurgical patients, three males, four females, ranging in age from 4.5 months to 70 years) that the CSF conductivity at body-temperature can accurately be measured to be 1.79 S/m with a maximal standard deviation of less than 1.4% between subjects for the large frequency range between 10Hz and 10,000Hz. Additionally, the CSF compartment was shown to have a significant influence on EEG source analysis (Ramon et al., 2004; Wendel et al., 2008; Rullmann et al., 2008). In four-compartment models, this layer is taken into account, but source eccentricity then has to

be determined with regard to the inner CSF surface, i.e., the most eccentric sources are only 1 or 2mm apart from the next conductivity discontinuity. Therefore, eccentricities of more than 98% have to be examined. It is well-known (and in (Wolters et al., 2007a), a theoretical reasoning was given for this fact), that with increasing eccentricity, the numerical accuracy decreases. This is not only the case for the subtraction approach (Bertrand et al., 1991; van den Broek, 1997; Marin et al., 1998; Schimpf et al., 2002; Wolters et al., 2007a), but also for the direct approaches in FE modelling (Yan et al., 1991; Buchner et al., 1997; Schimpf et al., 2002; Wolters et al., 2007b). Examining modelling accuracy at high source eccentricities is thus important and constitutes a major numerical challenge. In this paper, a four-compartment sphere model is used for validation of the proposed FE approach, the CSF compartment is modelled with the isotropic conductivity value of 1.79 S/m (Baumann et al., 1997) and sources are considered with eccentricities up to 98.7% (1mm below the CSF). Furthermore, as (Marin et al., 1998; Wolters et al., 2007a) have shown, modelling skull conductivity anisotropy is a further numerical challenge and generally leads to higher numerical errors than modelling the skull as an isotropic compartment. Following (Marin et al., 1998), we will model the skull compartment with a conductivity anisotropy of 1:10.

The numerical accuracy of a subtraction approach is determined by means of the following two important criteria: i) FE approach for the numerical computation of the correction potential and ii) FE mesh generation procedure. Until now, in 4 layer sphere model validation studies with realistic source eccentricities up to 98%, none of the presented FE approaches were shown to achieve satisfying numerical accuracy in combination with being practically feasible in an inverse source analysis scenario. The projected subtraction ap-

proach presented in (Wolters et al., 2007a) only performed well up to 95% eccentricity. (Schimpf et al., 2002) investigated an FE subtraction approach in a regular 1mm hexahedral model of a four layer sphere volume conductor with isotropic skull and sources up to 1mm below the CSF compartment. For the most eccentric source, a topography error of 7% and a magnitude error of 25% were reported. It is well-known also from other studies that the abrupt transitions and right angles of regular hexahedral models at material interfaces negatively influence especially the magnitude error (Wolters et al., 2007b). Even if a geometry-adaptation of the hexahedra can alleviate this problem (Wolters et al., 2007b), a well-chosen tetrahedralisation will still better represent smooth tissue boundaries and can furthermore be adapted to the specific structure of the solution function. However, until now, only *ordinary Delaunay tetrahedralisation* as defined in (Si and Gärtner, 2005; Si, 2008) was proposed for FE-based source analysis (Bertrand et al., 1991; van den Broek, 1997; Buchner et al., 1997; Marin et al., 1998; Wolters et al., 2007a). In (Bertrand et al., 1991; van den Broek, 1997; Marin et al., 1998), coarse ordinary tetrahedral meshes were considered yielding unacceptably large numerical errors already at eccentricities above 90%. In (Bertrand et al., 1991; van den Broek, 1997), local mesh refinement around the source was used to achieve better results. However, with regard to the inverse problem, the setup of source-location dependent locally refined meshes is difficult to implement and time-consuming to compute and thus might not be practicable for an inverse source analysis.

In this paper, we propose a so-called *full subtraction FE approach* which appropriately evaluates the right-hand side integral for the correction potential with the objective of achieving highest possible convergence order for linear

basis functions. A *constrained Delaunay tetrahedralisation* (CDT) approach will be presented and used for the generation of high-quality FE meshes. Even if we will also propose to adapt the tetrahedralisation by means of an appropriate refinement and coarsening to the correction potential solution function, our new approach does not need local mesh refinement around the source. As we will show, it therefore allows the construction of transfer matrices for fast computation of the inverse problem. We validate the new approach in a four-layer sphere model with highly-conductive CSF and anisotropic skull compartment and sources up to 1mm below the CSF compartment. We compare the accuracy of our new method with the projected subtraction approach from (Wolters et al., 2007a) and the literature. It will be shown that the combination of the full subtraction approach with the CDT-FE meshes leads to very low numerical errors for the computed EEG potentials. Note that since the magnetoencephalography (MEG) forward problem is also based on the computed electric potential (see, e.g., Hämäläinen et al. (1993); Wolters et al. (2004)), our method is directly applicable to MEG source analysis, too.

2 Methods

2.1 The Continuous Forward Problem

The mathematical model for the numerical simulation of electric and magnetic fields in the human head is based on the quasistatic approximation of Maxwell's equations (Plonsey and Heppner, 1967; Sarvas, 1987; Hämäläinen et al., 1993). Following (Sarvas, 1987; de Munck et al., 1988; Hämäläinen et al., 1993; Murakami and Okada, 2006), the primary current density function is de-

$$J^p = J^y, \quad J^y(x) = \operatorname{div} M(y)\delta(x-y), \qquad y \in Y \subset \Omega, \;\; M(y) \in \mathbb{R}^3 \tag{1}$$

with $M(y)$ being the current dipolar moment at position y, $\Omega \subset \mathbb{R}^3$ the head domain, Y the central surface of the gray matter compartment where the dipole sources are located (Y is thus the *source space*) and δ the Dirac delta distribution. The forward problem in source analysis is then to find a solution for the electric potential u (in an appropriate function space) such that

$$\begin{aligned} \operatorname{div} \sigma(x)\, \nabla u(x) &= J^p(x) \quad \text{for a.e. } x \in \Omega, \\ \langle \sigma(x) \nabla u(x), n(x) \rangle &= 0 \quad \text{for a.e. } x \in \Gamma, \\ \int_\Omega u(x) dx &= 0. \end{aligned} \tag{2}$$

with $\sigma(x)$ ($\sigma : \mathbb{R}^3 \to \mathbb{R}^{3\times 3}$) being the symmetric positive definite conductivity tensor at position x, $n(x)$ the outer unit normal at a scalp surface point $x \in \Gamma$ and $\langle \cdot, \cdot \rangle$ the inner product (a.e. is an abbreviation for *almost every*). In order to understand the difficulties of a discretisation of the forward problem we consider a simple example where the solution is known analytically. For an unbounded volume conductor $\Omega = \mathbb{R}^3$ and a constant homogeneous conductivity $\sigma(x) \equiv \sigma(y)$ for all $x \in \Omega$, the solution $u^{\infty,y}$ for the right-hand side $J^p = J^y$ of (2) is given by

$$u^{\infty,y}(x) := \frac{1}{4\pi\sqrt{\det \sigma(y)}} \frac{\langle M(y), \sigma(y)^{-1}(x-y) \rangle}{\langle \sigma(y)^{-1}(x-y), x-y \rangle^{3/2}}. \tag{3}$$

Later, we will also need the gradient of this function, which can be expressed as

$$\nabla u^{\infty,y}(x) = \frac{1}{4\pi\sqrt{\det \sigma(y)}} \cdot \frac{\sigma(y)^{-1} M(y)}{\langle \sigma(y)^{-1}(x-y), x-y \rangle^{3/2}} \tag{4}$$

$$-\frac{1}{4\pi\sqrt{\det\sigma(y)}}\cdot\frac{3\langle M(y),\sigma(y)^{-1}(x-y)\rangle\sigma(y)^{-1}(x-y)}{\langle\sigma(y)^{-1}(x-y),x-y\rangle^{5/2}}.$$

Further properties of this so-called *singularity potential* function $u^{\infty,y}$ are given in Appendix A.1. In order to resolve the singularity of $u^{\infty,y}$ at $x = y$ in the discretisation, one would have to include special singular basis functions or use a locally refined grid. In the following, we will derive a continuous formulation where the singularity in the right-hand side is removed so that standard discretisation techniques are applicable.

2.2 Subtraction forward problem

In order to apply a finite element discretisation, we have to reformulate the problem, because neither the right-hand side J^p nor the solution u allow for a good approximation by standard finite elements. Moreover, the variational formulation would require an integration by parts (Gauß integral theorem, resp. Green's identity), which might not be applicable for singular functions such as the solution for the total potential u and the right-hand side J^p from equation (2). Therefore, with $u^{\infty,y}$ being the singularity potential from (3), the *subtraction forward problem* is to find a solution for the *correction potential*, $u^{\mathrm{corr,y}}$, (in an appropriate function space) such that

$$\begin{aligned}\operatorname{div}\sigma(x)\,\nabla(u^{\mathrm{corr,y}}(x)+u^{\infty,y}(x)) &= J^p(x) \quad \text{for a.e. } x\in\Omega,\\ \langle\sigma(x)\nabla(u^{\mathrm{corr,y}}(x)+u^{\infty,y}(x)),n(x)\rangle &= 0 \quad \text{for a.e. } x\in\Gamma,\\ \int_\Omega (u^{\mathrm{corr,y}}(x)+u^{\infty,y}(x))dx &= 0.\end{aligned} \tag{5}$$

Equation (5) can be written in the form

$$\operatorname{div}\sigma(x)\,\nabla u^{\mathrm{corr,y}}(x) = f(x) \ \text{ for a.e. } x\in\Omega, \tag{6}$$

$$\langle \sigma(x)\nabla u^{\mathrm{corr,y}}(x), n(x)\rangle = g(x) \quad \text{for a.e. } x \in \Gamma, \tag{7}$$
$$\int_\Omega u^{\mathrm{corr,y}}(x)dx = -\int_\Omega u^{\infty,y}(x)dx,$$

with the right-hand side functions

$$f(x) := \mathrm{div}\ (\sigma(y) - \sigma(x))\ \nabla u^{\infty,y}(x) \quad \text{for } x \in \Omega, \tag{8}$$
$$g(x) := -\langle \sigma(x)\nabla u^{\infty,y}(x), n(x)\rangle \text{ for } x \in \Gamma. \tag{9}$$

In source analysis, the human cortex is most often assumed to be isotropic (Bertrand et al., 1991; van den Broek, 1997; Schimpf et al., 2002; Kybic et al., 2005). This assumption was recently confirmed by (Shimony et al., 1999), who measured water diffusion anisotropy in 12 regions of interest in the human brain and found the cortex to be an isotropic compartment [1]. We will therefore in the following assume isotropic conductivity for the cortical layer. However, even in case of cortical anisotropy, a so-called *homogeneity assumption*, needed for the subtraction approach, is very reasonable. It assumes that a small subdomain Ω_ϵ^y can be found around any source position $y \in Y$ such that the tensor $\sigma(x)$ is homogeneous (isotropic or anisotropic) for all $x \in \Omega_\epsilon^y$ (see Assumption 1 in Appendix A.2). In case of cortical anisotropy, Ω_ϵ^y might, e.g., be a voxel (at least a subdomain of a voxel) for which a conductivity tensor was determined indirectly from measured diffusion tensor magnetic resonance imaging (Tuch et al., 2001; Wang et al., 2008). Because of the homogeneity assumption, we find $\sigma(y) - \sigma(x) = 0$ for all $x \in \Omega_\epsilon^y$, so that in subdomain Ω_ϵ^y, where u^∞ is singular, the right-hand side function $f(x)$ in equation (6) is

[1] This assumption was furthermore approved by world experts in DTI on the 2nd International Summer School about Diffusion Tensor Magnetic Resonance Imaging, Institute for Biomedical Engineering, University of Ilmenau, Germany, http://www.tu-ilmenau.de/fakia/Summerschool-2007.7753.0.html?&no_cache=1.

identical to zero. The singularity on the right-hand side of equation (5) was thus successfully eliminated by means of the subtraction approach and the right-hand side function $f(x)$ in equation (6) is now square-integrable over the whole domain Ω and thus appropriate for a finite element approach. Additionally, for existence and uniqueness of a solution for the elliptic differential equation (6) with inhomogeneous Neumann boundary condition (7) and right-hand side functions (8) and (9), a *compatibility condition* has to be fulfilled, which will be proved in Lemma 2 (see Appendix A.2). Therefore, the problem is well defined and appropriate for a variational formulation (Hackbusch, 1992; Braess, 2007), which will be derived in Appendix A.3.

2.3 Finite element approach

For the subtraction forward problem, the variational formulation and the Galerkin finite element approach using standard conforming linear basis functions φ_i at nodal positions ξ_i $(i = 1, \ldots, N)$ is presented in Appendix A.3.

2.3.1 Numerics of the full subtraction approach

The finite element approach leads to the following linear system for the *full subtraction approach*:

$$Ku = b^y, \quad K \in \mathbb{R}^{N\times N},\ u, b^y \in \mathbb{R}^N \tag{10}$$

with the stiffness matrix

$$K_{i,j} := \int_\Omega \langle \sigma(x)\nabla\varphi_j, \nabla\varphi_i\rangle dx, \quad i,j = 1,\ldots,N \tag{11}$$

and the right-hand side

$$b_i^y := \int_\Omega \langle (\sigma(y) - \sigma(x)) \nabla u^{\infty,y}(x), \nabla \varphi_i(x) \rangle dx \tag{12}$$

$$- \int_\Gamma \varphi_i(x) \langle n(x), \sigma(y) \nabla u^{\infty,y}(x) \rangle dx, \quad i = 1, \ldots, N. \tag{13}$$

The term $\nabla \varphi_i$ is constant for linear elements, so that entries of K in (11) can be computed easily. The entries of the right-hand side b^y need to be accurate enough in order to preserve the finite element convergence. The gradient of $u^{\infty,y}$ can be computed analytically following equation (4). Since we project the correction potential into the space of piecewise linear elements, it is sufficient to have a perturbation of an order of the square of the step size which is achieved by a second order accurate quadrature formula. In Section 3.1 we will verify that this order is necessary and sufficient to produce a negligible quadrature error. We assemble the first term (12) of b_i^y element-wise. For $x \to y$, the integral even vanishes because of the homogeneity assumption. The second term (13) involves the normal vector and the basis function itself. Thus, we need a quadrature formula that resolves $\nabla u^{\infty,y}$ at the boundary (where it is very smooth) and that is accurate for linear functions. Again, a second order quadrature formula for the surface triangles is necessary and sufficient, as will be verified in Section 3.1.

Please put Table 1 here.

For the numerical integration of the right-hand side (12), (13), we use quadrature formulas of (Stroud, 1971). As shown in Table 1, the overall numerical accuracy of the full subtraction approach will be evaluated for quadrature orders of 1, 2 and 7. Our notation in Table 1 closely follows the one of the

tables in (Stroud, 1971). T_n indicates an n-dimensional simplex (Stroud, 1971, Chapter 7.8) (in our case: $n = 3$).

2.3.2 Numerics of the projected subtraction approach

In (Wolters et al., 2007a), a *projected subtraction approach* was presented where the function $u^{\infty,y}$ is projected in the finite element space by

$$u^{\infty}(x) \approx u_N^{\infty}(x) = \sum_{j=1}^{N} \varphi_j(x) u_j^{\infty}, \quad u_j^{\infty} = u^{\infty}(\xi_j). \tag{14}$$

Introducing the coefficient vector $u_\infty := (u_1^\infty, \ldots, u_N^\infty)$, the system of equations

$$Ku = -K^{corr} u_\infty - S u_\infty \tag{15}$$

was obtained where K was defined in (11) and the matrices K^{corr} and S are defined by

$$K_{i,j}^{corr} := -\int_{\Omega} \langle (\sigma(y) - \sigma(x)) \nabla\varphi_j(x), \nabla\varphi_i(x) \rangle dx \tag{16}$$

and

$$S_{i,j} := \int_{\partial\Omega} \langle \sigma(y) \nabla\varphi_j(x), n(x) \rangle \varphi_i(x) dx. \tag{17}$$

Even if the projected subtraction approach is computationally less expensive because for each source, only the coefficient vector u_∞ has to be computed, the drawback of the approach is the additional approximation error by (14). We will see in the numerical validation section that the presented full subtraction approach in which u^∞ is not approximated in the FE space has a much higher degree of accuracy.

Fast transfer matrices are needed to strongly reduce computational complexity with regard to FE based inverse EEG and MEG source analysis (Gencer and Acar, 2004; Wolters et al., 2004; Pursiainen, 2007, 2008; Calvetti et al., 2008). In Appendix A.4 we will show that only for the full subtraction approach, a fast transfer matrix approach can be derived for both cortical conductivity isotropy as well as anisotropy, whereas for the projected subtraction approach, a fast transfer matrix approach implies an isotropic cortical compartment. In Appendix A.5, we will furthermore present efficient concepts for precomputing lead field matrices that are needed for a large class of inverse source analysis methods.

2.5 Validation platform

2.5.1 Analytical solution in an anisotropic multilayer sphere model

De Munck and Peters (de Munck and Peters, 1993) derived series expansion formulas for a mathematical dipole in a multilayer sphere model, denoted here as the "analytical solution". A rough overview of the formulas will be given in this section. The model consists of S shells with radii $r_S < r_{S-1} < \ldots < r_1$ and constant radial, $\sigma^{\mathrm{rad}}(r) = \sigma_j^{\mathrm{rad}} \in \mathbb{R}^+$, and constant tangential conductivity, $\sigma^{\mathrm{tang}}(r) = \sigma_j^{\mathrm{tang}} \in \mathbb{R}^+$, within each layer $r_{j+1} < r < r_j$. It is assumed that the source at position x_0 with radial coordinate $r_0 \in \mathbb{R}$ is in a more interior layer than the measurement electrode at position $x_e \in \mathbb{R}^3$ with radial coordinate $r_e = r_1 \in \mathbb{R}$. The spherical harmonics expansion for the mathematical dipole (1) is expressed in terms of the gradient of the monopole potential to the

source point. Using an asymptotic approximation and an addition-subtraction method to speed up the series convergence yields

$$\mathrm{u_{ana}}(x_0, x_e) = \frac{1}{4\pi}\langle \mathbf{M}, S_0 \frac{x_e}{r_e} + (S_1 - \cos\omega_{0e} S_0)\frac{x_0}{r_0}\rangle$$

with ω_{0e} being the angular distance between source and electrode, and with

$$\begin{aligned} S_0 = & \frac{F_0}{r_0}\frac{\Lambda}{(1 - 2\Lambda\cos\omega_{0e} + \Lambda^2)^{3/2}} \\ & + \frac{1}{r_0}\sum_{n=1}^{\infty}\left\{(2n+1)R_n(r_0, r_e) - F_0\Lambda^n\right\} P_n'(\cos\omega_{0e}) \end{aligned} \tag{18}$$

and

$$\begin{aligned} S_1 = & F_1\frac{\Lambda\cos\omega_{0e} - \Lambda^2}{(1 - 2\Lambda\cos\omega_{0e} + \Lambda^2)^{3/2}} \\ & + \sum_{n=1}^{\infty}\left\{(2n+1)R_n'(r_0, r_e) - F_1 n\Lambda^n\right\} P_n(\cos\omega_{0e}). \end{aligned} \tag{19}$$

The coefficients R_n and their derivatives, R_n', are computed analytically and the derivative of the Legendre polynomials, P_n, are determined by means of a recursion formula. We refer to (de Munck and Peters, 1993) for the derivation of the above series of differences [2] and for the definition of F_0, F_1 and Λ. Here, it is only important that the latter terms are independent of n and that they can be computed from the given radii and conductivities of layers between source and electrode and of the radial coordinate of the source. The computations of the series (18) and (19) are stopped after the k-th term, if

[2] The following is a result of a discussion with J.C. de Munck: While constants in formulas (71) and (72) in the original paper (de Munck and Peters, 1993) have to be flipped, our versions of S_0 and S_1 in Equations (18) and (19) are correct.

the following criterion is fulfilled

$$\frac{t_k}{t_0} \leq \upsilon, \qquad t_k := (2k+1)R'_k - F_1 k \Lambda^k. \tag{20}$$

In the following simulations, a value of 10^{-6} is chosen for υ in (20). Using the asymptotic expansion, no more than 30 terms are needed for the series computation at each electrode.

2.5.2 Error criteria

We will compare numerical solutions with analytical solutions using three error criteria that are commonly evaluated in source analysis (Meijs et al., 1989; Bertrand et al., 1991; van den Broek, 1997; Marin et al., 1998; Schimpf et al., 2002; Wolters et al., 2007a). The *relative (Euclidean) error* (RE) is defined as

$$\mathrm{RE} = ||\underline{\mathrm{u}}^{\mathtt{num}} - \underline{\mathrm{u}}^{\mathtt{ana}}||_2 / ||\underline{\mathrm{u}}^{\mathtt{ana}}||_2,$$

where $\underline{\mathrm{u}}^{\mathtt{ana}}, \underline{\mathrm{u}}^{\mathtt{num}} \in \mathbb{R}^{\mathrm{m}}$ denote the analytical and the numerical solution vector, resp., at m measurement electrodes. In order to better distinguish between the topography (driven primarily by changes in dipole location and orientation) and the magnitude error (indicating changes in source strength), (Meijs et al., 1989) introduced the *relative difference measure* (RDM)

$$\mathrm{RDM} = \sqrt{\sum_{i=1}^{\mathrm{m}} \left(\underline{\mathrm{u}}_i^{\mathtt{ana}} / ||\underline{\mathrm{u}}^{\mathtt{ana}}||_2 - \underline{\mathrm{u}}_i^{\mathtt{num}} / ||\underline{\mathrm{u}}^{\mathtt{num}}||_2\right)^2}$$

(for zero-mean data holds $0 \leq \mathrm{RDM} \leq 2$ (Schimpf et al., 2002)) and the *magnification factor* (MAG)

$$\mathrm{MAG} = ||\underline{\mathrm{u}}^{\mathtt{num}}||_2 / ||\underline{\mathrm{u}}^{\mathtt{ana}}||_2$$

(minimal error: MAG = 1), respectively.

2.5.3 Four compartment anisotropic sphere model

Please put Table 2 here.

The validation of the presented full subtraction approach will be carried out in a four compartment sphere model with anisotropic skull compartment, whose parameterisation is shown in Table 2.

The numerical forward solution is validated by means of the corresponding analytic solution for dipoles located on the y-axis at depths of 0% to 98.7% (in 1mm steps) of the brain compartment (78mm radius) using both radial and tangential dipole orientations. *Eccentricity* is defined here as the percent ratio of the distance between the source location and the model midpoint divided by the radius of the inner sphere (78mm radius). The most eccentric source considered is thus only 1mm below the CSF compartment. Tangential sources are oriented in the $+z$-axis and radial dipoles in the $+y$-axis. The dipole amplitudes are chosen to be 1nAm.

To achieve error measures which are independent of the specific choice of the sensor configuration, we distributed electrodes in a most-regular way over a given sphere surface. In this way we generated a 748 electrode configuration on the surface of the outer sphere.

The FE meshes of the four layer sphere model were generated by the software TetGen (Si, 2004) which uses a *constrained Delaunay tetrahedralisation* (CDT) approach (Si and Gärtner, 2005; Si, 2008). The meshing procedure started with the preparation of a suitable boundary discretisation of the model. To begin with, for each of the four layers and for a given triangle edge length, nodes were distributed in a most-regular way and connected through triangles. This yielded a valid triangular surface mesh for each of the four layers. Meshes of different layers were not intersecting each other. The CDT approach was then used to construct a tetrahedralisation conforming to the surface meshes. It first built a Delaunay tetrahedralisation of the vertices of the surface meshes. It then used a local degeneracy removal algorithm combining vertex perturbation and vertex insertion to construct a new set of vertices which included the input set of vertices. In the last step, a fast facet recovery algorithm was used to construct the CDT (Si and Gärtner, 2005; Si, 2008).

This approach is combined with two further constraints to the size and shape of the tetrahedra. The first constraint can be used to restrict the volume of the generated tetrahedra in a certain compartment, the so-called *volume constraint*. The second constraint is important for the generation of quality tetrahedra. If R denotes the radius of the unique circumsphere of a tetrahedron and L its shortest edge length, the so-called *radius-edge ratio* of the tetrahedron can be defined as

$$Q = \frac{R}{L}.$$

The radius-edge ratio can detect almost all badly-shaped tetrahedra except

one type of tetrahedra, so-called *slivers*. A sliver is a very flat tetrahedron which has no small edges, but can have arbitrarily large dihedral angles (close to π). For this reason, an additional mesh smoothing and optimization step was used to remove the slivers and improve the overall mesh quality.

Please put Table 3 here.

In Table 3, the number of nodes and elements of the three tetrahedral meshes are shown which will be used for numerical accuracy tests.

Please put Figure 1 here.

The tetrahedral mesh `tet360K` of the four compartment sphere model is shown in Figure 1. For this model, we distributed 31,680 nodes on each of the four surfaces for the CDT procedure. We allowed for a maximal radius-edge ratio of $Q = 1.2$. The volumes of the tetrahedra in the compartments skin, skull and CSF were furthermore restricted correspondingly to the chosen surface triangle edge length. As it can be observed in Figure 1, no volume constraint was used for the brain layer since for this compartment, the entries of the volume integral (12) are zero ($(\sigma(y) - \sigma(x)) = 0$ for all x in the brain compartment) so that a coarse resolution will not spoil the overall numerical accuracy, but reduce the computational amount of work.

2.5.5 FE solver method.

We employ an algebraic multigrid preconditioned conjugate gradient (AMG-CG) method for solving the linear systems (10) and (15). We solve up to

a relative error of 10^{-8} in the controllable $KN^{-1}K$-energy norm (with N^{-1} being one V-cycle of the AMG) (Wolters et al., 2002; Haase et al., 2002).

3 Results

3.1 Evaluation with regard to right-hand side quadrature order

Please put Figure 2 here.

In the first study, we compared the numerical accuracy of the presented full subtraction approach for quadrature formulas with different integration order for the right-hand side (12), (13). The goal of this study was to verify that second order integration formulas are necessary and sufficient as stated in Section 2.3. Figure 2 shows the relative errors between the numerical and the quasi-analytical solutions for tangential (left column) and radial sources (right column) for the models `tet39K` (top row), `tet287K` (middle row) and `tet360K` (bottom row) from Table 3. The different quadrature orders of 1, 2 and 7 are represented with different colors and labels in the figure. Especially for eccentric sources, the integration order 1 performed worse than order 2. This shows the necessity of second order integration. Second order integration was also sufficient since the difference between order 2 and 7 in Figure 2 is not visible (models `tet287K` and `tet360K`) or very small (model `tet39K`) and, in any case, not worth the much larger computational amount of work for the higher quadrature order.

Please put Figure 3 here.

Please put Figure 4 here.

In the second study, we evaluated the numerical errors with regard to the resolution of the FE discretisation. Following the results of Section 3.1, a quadrature order of 2 was used for the integration of the right-hand side. Figure 3 shows the RE for the three models of Table 3 for tangentially (left) and radially oriented dipoles (right). A clear convergence can be observed, i.e., the RE decreases over all eccentricities with increasing mesh resolution. The accuracy increase is especially distinct for eccentric sources. With the finest model `tet360K`, we were able to decrease the maximal RE over all eccentricities and source orientations to a value of 0.71% for the most eccentric radial source 1mm below the CSF compartment. Figure 4 shows the corresponding RDM and MAG errors for the finest model `tet360K`. The largest topography error is an RDM of 0.34% and the largest magnitude error a MAG of 0.3%.

3.3 Comparison of projected and full subtraction approach

Please put Figure 5 here.

In a last study, we compared the presented full subtraction approach with the projected subtraction method from (Wolters et al., 2007a). Figure 5 shows

the RE for tangential (left column) and radial sources (right column) for the models `tet39K` (top row), `tet287K` (middle row) and `tet360K` (bottom row) from Table 3. It can be summarized that the presented full subtraction approach is a major step forward with regard to accuracy for all examined mesh resolutions, which is especially prominent for eccentric sources. For the finest model `tet360K` (bottom row), the largest RE of 5% for the projected subtraction approach was reduced by more than a factor of 7 to a maximal RE of 0.71% for the presented full subtraction approach.

4 Discussion and conclusion

We presented theory and numerical experiments of a full subtraction approach to model a mathematical dipole in finite element (FE) method based electroencephalography (EEG) source reconstruction using constrained Delaunay tetrahedral (CDT) meshes. Since the magnetoencephalography (MEG) forward problem is also based on the computed electric potential (see, e.g., (Hämäläinen et al., 1993; Wolters et al., 2004)), our method is directly applicable to MEG source analysis. We embedded the approach for the computation of the correction potential in the general FE convergence theory and found that under the assumption of higher regularity, it is important to integrate the right-hand side of the FE approach for the correction potential with a quadrature order of 2 for achieving highest possible accuracy.

We validated our implementation of the method in a four-compartment sphere model. We used the conductivity value of 1.79 S/m for the cerebrospinal fluid (CSF) compartment as measured for human CSF at body-temperature by (Baumann et al., 1997). The importance of modelling the CSF with regard to

source analysis was shown by (Ramon et al., 2004; Wendel et al., 2008; Rullmann et al., 2008). Modelling the CSF necessitates the examination of numerical accuracies for sources with very high eccentricities, because the sources in the grey matter compartment are then only 1 or 2mm apart from the next conductivity discontinuity. This constitutes a major numerical challenge. Following (Marin et al., 1998), we furthermore modelled the skull compartment as a 1:10 anisotropic conductor. It is also well-known that modelling skull anisotropy is a further numerical challenge and generally leads to higher numerical errors than modelling the skull as an isotropic compartment (Marin et al., 1998; Wolters et al., 2007a). In the numerical experiments, we found that second order integration is necessary and sufficient, as the theory also predicts. Our new approach was shown to converge, i.e., with increasing mesh size, numerical errors decreased. The evaluation of the convergence order is a difficult task because the convergence constant is strongly depending on the distance of the source to the next conductivity discontinuity (a theoretical reasoning for this fact is given in (Wolters et al., 2007a)). With regard to the EEG inverse problem, an evaluation of the numerical accuracy at the surface electrodes seems to be sufficient, as also done by others (Bertrand et al., 1991; van den Broek, 1997; Awada et al., 1997; Marin et al., 1998; Schimpf et al., 2002; Kybic et al., 2005; Hallez et al., 2005). We therefore evaluated the numerical accuracy of the new approach at 748 surface points over all source eccentricities for sources up to 1mm below the CSF compartment. We consider it to be very progressive that, for the finest of the examined high-quality CDT FE meshes with 360K nodes which was not locally refined around the source singularity (the meshing approach can thus be used for inverse source analysis scenarios) and for the maximal examined source eccentricity of 98.7%, the full

subtraction method yielded

- a maximal relative error (maxRE) of 0.71%,
- a maximal relative difference measure (maxRDM) of 0.34%,
- and a maximal magnification factor (maxMAG) of 0.3%.

In a direct comparison with the projected subtraction approach from (Wolters et al., 2007a), we found that the new method is by an order of magnitude more accurate for dipole sources close to the next conductivity discontinuity. The fact that, in a realistic head model, most sources of interest have eccentricities between 50% and 98% shows the importance of our results. A direct comparison of our approach with other studies from the literature is difficult since the setups are never identical. We however in the following collect the major results of similar studies. (Schimpf et al., 2002) investigated an FE subtraction approach in a four layer sphere model with isotropic skull and sources up to 1mm below the CSF compartment. In their article, a regular 1mm cube model was used (thus a much higher FE resolution) and a maxRDM of 7% and a maxMAG of 25% was achieved. Especially because of limited computational power, older studies generally use much coarser models. In a locally refined (around the source singularity) tetrahedral mesh with 12,500 nodes of a four layer sphere model with anisotropic skull and first order FE basis functions, (Bertrand et al., 1991) reported numerical accuracies up to a maximal eccentricity of 97.6%. A maximal RDM of above 20% and a maximal MAG up to 70% were documented for the most eccentric source. (van den Broek, 1997) also used a locally refined (around the source singularity) tetrahedral mesh with 3,073 nodes of a three layer sphere model with anisotropic skull. For the maximal examined eccentricity of 94.2%, an RDM of up to 50% was given. It was mentioned in the conclusion that in some cases the accuracy could not

further be improved by adding points globally as the numerical stability of the matrix equation that had to be solved was reduced. (Marin et al., 1998) used second order FE basis functions, but their finest tetrahedral mesh of 87,907 nodes was restricted to eccentricities of 81% in order to reach a sufficient accuracy for radial dipole forward solutions in a three compartment sphere model with anisotropic skull. (Awada et al., 1997) implemented a 2D subtraction approach and compared its numerical accuracy with a direct potential method in a 2D sphere model. A direct comparison with our results is therefore especially difficult, but the authors concluded that the subtraction method was generally more accurate than the direct approach.

Besides its higher accuracy, the possibility of also modelling cortical anisotropy in combination with the efficient FE transfer matrix approach might be a further advantage of the full subtraction approach when compared to the projected subtraction approach from (Wolters et al., 2007a). The infant grey matter is sometimes referred to be a slightly anisotropic conductor because of yet less developed synaptic connections to the cortical pyramidal cells. However, DTI measurements show that the grey matter in adults is isotropic (Shimony et al., 1999), being one reason for our study (besides the possibility to better embed our results into the literature) to evaluate numerical errors for isotropic cortical compartments.

As a final note, instead of trying to reduce numerical errors for the probably "over-singular" mathematical point dipole that is most often used in source analysis, it is important to reconsider other and especially smoother source models, taking into account the fact that the primary current sources are continuous throughout the cortical tissue (Tanzer et al., 2005; Pursiainen, 2007; Wolters et al., 2007b; Pursiainen, 2008; Calvetti et al., 2008). This is

where the FE-based subtraction method might provide a further important contribution to EEG and MEG source analyses.

A Detailed mathematics

A.1 The Continuous Forward Problem

Function $u^{\infty,y}$ from equation (3) fulfils the Neumann boundary conditions at infinity ($x \to \infty$). The singularity of $u^{\infty,y}$ at $x = y$ is of order 2, so that $u^{\infty,y}$ does not belong to the Sobolev-space $H^1(\Omega)$ (this function space only contains functions which are square-integrable and whose first weak derivative is also square-integrable), not even to $L^2(\Omega)$ (the space of square-integrable functions). However, $u^{\infty,y}$ belongs to $L^1(\Omega)$, i.e., it is integrable. Refer, e.g., to (Hackbusch, 1992; Braess, 2007) for a more detailed definition of the function spaces.

A.2 Subtraction forward problem

In order to remove the singularities in the right-hand side of (6), the following assumption is needed for the subtraction approach:

Assumption 1 (Homogeneity assumption) *Let $\epsilon > 0$ such that for every $y \in Y$, the tensor $\sigma(x)$ is homogeneous (isotropic or anisotropic) in a small subdomain*

$$\Omega_\epsilon^y := \{x \in \Omega \mid \|x - y\|_2 < \epsilon\} \subset \Omega \tag{A.1}$$

As described in Section 2.2, the homogeneity assumption is valid for every $y \in Y$, i.e., for every possible source in the human cortex compartment.

Additionally, for existence and uniqueness of a solution for the elliptic differential equation (6) with inhomogeneous Neumann boundary conditions (7), the *compatibility condition*

$$\int_{\Omega} f d\Omega - \int_{\Gamma} g d\Gamma = 0 \tag{A.2}$$

has to be fulfilled. This condition results from Gauß' theorem, since it is

$$\int_{\Omega} f d\Omega \overset{(6)}{=} \int_{\Omega} \operatorname{div}\ (\sigma \nabla u^{\mathrm{corr,y}})\, d\Omega \overset{\text{Gauß}}{=} \int_{\Gamma} \langle \sigma \nabla u^{\mathrm{corr,y}}, \mathrm{n} \rangle d\Gamma \overset{(7)}{=} \int_{\Gamma} g d\Gamma.$$

The next Lemma will prove the compatibility condition.

Lemma 2 (Compatibility) *The differential equation (6) with inhomogeneous Neumann boundary condition (7) fulfils the compatibility condition (A.2).*

Proof: Let us define $\Omega' := \Omega \setminus \Omega_\epsilon^y$ and let $\Gamma_\epsilon^y = \partial \Omega_\epsilon^y$ be the surface of the spherical domain Ω_ϵ^y that was defined in (A.1). We then get

$$\begin{aligned}
&\int_{\Omega} f(x) - \int_{\Gamma} g(x) \\
\overset{(8,9)}{=}\ &\int_{\Omega} \operatorname{div}\ (\sigma(y) - \sigma(x))\ \nabla u^{\infty,y}(x) + \int_{\Gamma} \langle \sigma(x) \nabla u^{\infty,y}(x), n(x) \rangle \\
\overset{\text{Gauß}}{=}\ &\int_{\Gamma} \langle (\sigma(y) - \sigma(x)) \nabla u^{\infty,y}(x), \mathrm{n}(x) \rangle + \int_{\Gamma} \langle \sigma(x) \nabla u^{\infty,y}(x), n(x) \rangle \\
=\ &\int_{\Gamma} \langle \sigma(y) \nabla u^{\infty,y}(x), \mathrm{n}(x) \rangle
\end{aligned}$$

$$\begin{aligned} &\overset{\text{Gauß}}{=} \int_{\Omega'} \operatorname{div}\ (\sigma(y)\nabla u^{\infty,y}(x)) - \int_{\Gamma_\epsilon^y} \langle \sigma(y)\nabla u^{\infty,y}(x), \mathrm{n}(x)\rangle \\ &= \ 0. \end{aligned}$$

In the last step, both integrals are zero: The volume integral is zero, because $u^{\infty,y}$ is a solution of the homogeneous problem (2) and $J^p(x) = 0$ for all $x \in \Omega'$.

The surface integral is zero, since $u^{\infty,y}$ is the potential for a dipole in the midpoint of the spherical integration domain Ω_ϵ^y and, if we divide the surface Γ_ϵ^y into the upper part $(\Gamma_\epsilon^y)^+$ and the lower part $(\Gamma_\epsilon^y)^-$, it can be seen that the surface integral over $(\Gamma_\epsilon^y)^-$ is exactly the negative of the surface integral over $(\Gamma_\epsilon^y)^+$. To show this, let $\mathrm{x}^- \in (\Gamma_\epsilon^y)^-$ and let $\mathrm{x}^+ \in (\Gamma_\epsilon^y)^+$ be the corresponding mirror point such that $\mathrm{x}^- - \mathrm{y} = -(\mathrm{x}^+ - \mathrm{y})$. We then have $\mathrm{n}(\mathrm{x}^-) = -\mathrm{n}(\mathrm{x}^+)$. From formula (4), we see that $\nabla u^{\infty,y}(\mathrm{x}^-) = \nabla u^{\infty,y}(\mathrm{x}^+)$. Therefore, we find

$$\int_{(\Gamma_\epsilon^y)^-} \langle \sigma(y)\nabla u^{\infty,y}(\mathrm{x}^-), \mathrm{n}(\mathrm{x}^-)\rangle = - \int_{(\Gamma_\epsilon^y)^+} \langle \sigma(y)\nabla u^{\infty,y}(\mathrm{x}^+), \mathrm{n}(\mathrm{x}^+)\rangle.$$

■

A.3 Variational formulation and finite element approach

Assumption 3 *Let $V \subset H^1(\Omega)$ be an infinite space and let $V_N \subset V$ be an N-dimensional subspace of V.*

The role of V_N is that of a finite element space, e.g. piecewise polynomials up to a certain degree. However, the space V might, due to higher regularity assumptions, be $H^{1+\varepsilon}(\Omega)$ with $\varepsilon \in]0,1[$, which is a subspace of $H^1(\Omega)$, i.e., $H^{1+\varepsilon}(\Omega) \subset H^1(\Omega)$.

Because of the smoothness of the functions in equations (6) and (7), we can now apply the Gauß integral theorem

$$\int_\Omega v(x)\mathrm{div}\sigma(x)\nabla u(x)dx = -\int_\Omega \langle \nabla v(x), \sigma(x)\nabla u(x)\rangle dx + \int_\Gamma v(x)\langle n(x), \sigma(x)\nabla u(x)\rangle dx$$

and arrive at the variational formulation that is suitable for a finite element discretisation.

Definition 4 (Analytical forward problem) *For an arbitrary mapping* $\alpha : \Omega \to \mathbb{R}^{3\times 3}$ *we define the bilinear form*

$$a_\alpha : V \times V \to \mathbb{R}, \quad a_\alpha(u,v) := \int_\Omega \langle \alpha(x)\nabla u(x), \nabla v(x)\rangle dx.$$

The weak formulation of the analytical forward problem (Equations (6) and (7)) is to find $u^{corr,y} \in V$ *s.t. for all* $v \in V$

$$a_\sigma(u^{corr,y}, v) = a_{\sigma(y)-\sigma}(u^{\infty,y}, v) - \int_{\partial\Omega} v(x)\langle n(x), \sigma(y)\nabla u^{\infty,y}(x)\rangle dx,$$
$$\int_\Omega u^{corr,y}(x)dx = -\int_\Omega u^{\infty,y}(x)dx.$$

In (Wolters et al., 2007a, Section 3.5), it is shown that a unique solution of the analytical forward problem exists and the solution $u^{corr,y}$ belongs to $H^1(\Omega)$.

Let $\tau = \{\tau_1, \ldots, \tau_T\}$ be a triangulation of the polygonal domain Ω into tetrahedra τ_i. For the finite element space V_N we use standard conforming linear elements, i.e. $V_N = \{v \in V \mid v|_{\tau_i} \text{ affine }, i = 1, \ldots, T\}$. Let $\mathrm{span}\,\{\varphi_i \mid i \in \mathcal{I}\}$ denote the standard Lagrange basis of V_N using local basis functions φ_i, $i \in \mathcal{I}, \#\mathcal{I} = N$. By ξ_i we denote the Lagrange point of the FE basis function

Definition 5 (Finite element forward problem) *The finite element forward problem is to find $u_N \in V_N$ s.t. for all $v \in V_N$*

$$a_\sigma(u_N, v) = a_{\sigma(y)-\sigma}(u^{\infty,y}, v) - \int_\Gamma v(x)\langle n(x), \sigma(y)\nabla u^{\infty,y}(x)\rangle dx,$$
$$\int_\Omega u_N(x)dx = -\int_\Omega u^{\infty,y}(x)dx.$$

This leads to the large sparse linear equation system (10).

A.4 Transfer matrix

For the inverse problem in EEG and MEG source analysis, the forward problem has to be solved for many right-hand sides $J^p = J^y$, $y \in Y$ (most often several thousands). In this case, the following assumption is necessary for an efficient computation of all solutions.

Assumption 6 *We demand that the FE mesh is the same for all right-hand sides $J^p = J^y$, i.e., we want to avoid local mesh refinement with regard to a specific source location.*

With regard to the EEG and MEG inverse problem, the full solution vector for the potential is not required for all right-hand sides. Instead, only a linear transform of the function u,

$$Au \in \mathbb{R}^m, \qquad m \ll N, \quad A : V \to \mathbb{R}^m,$$

is of interest with m being the number of (non-reference) measurement sensors.

In this case, one can precompute the so-called *transfer matrix*

$$T := \hat{A}K^{-1} \in \mathbb{R}^{m \times N}$$

where $\hat{A}$ is the matrix representation of the linear mapping A restricted to the finite dimensional space V_N in the basis $\{\varphi_i \mid i \in \mathcal{I}\}$ (Wolters et al., 2004) [3]. In case of the EEG, $\hat{A}$ is either a restriction or a surface interpolation of the potential vector to those FE nodes which represent the EEG electrodes. In case of the MEG, $\hat{A}$ is the secondary flux integration matrix (Wolters et al., 2004).

The full subtraction method EEG forward solution is thus obtained by

$$Au \approx A(u_N + u^{\infty,y}) = \hat{A}K^{-1}b^y + \hat{A}u^{\infty,y} = Tb^y + \hat{A}u^{\infty,y},$$

a matrix-vector multiplication with the $m \times N$ transfer matrix T. The MEG forward solution can exploit the precomputed MEG transfer matrix in a very similar fashion for the secondary magnetic flux parts (Wolters et al., 2004). The setup of the transfer matrix T requires m times the solution of an $N \times N$ linear equation system with the stiffness matrix K. Using an optimal method, e.g., multigrid, this can be done in $\mathcal{O}(m \cdot N)$ (Hackbusch, 1994, Theorem 10.4.2). The term $\hat{A}u^{\infty,y}$ can be computed easily because the solution $u^{\infty,y}$ is given analytically and it is smooth at the boundary where the support of $\hat{A}$ typically lies.

The projected subtraction approach (Wolters et al., 2007a) leads to the transfer matrix $\hat{A}K^{-1}(-K^{corr} - S)$. This approach is only useful, if all right-hand

[3] The transfer matrix is called *lead field basis* in (Wolters et al., 2004)

sides J^y have the same conductivity at all possible cortical source positions. This means that for the projected subtraction approach, $\sigma(y) = \sigma_c$ with an isotropic σ_c has to be assumed to allow for the use of the fast transfer matrix approach because the entries of the matrices K^{corr} and S in equations (16), (17) depend on the conductivity at the dipole position. In contrast, the conductivity for different source positions might vary for the presented full subtraction approach. This is a further advantage of the full subtraction approach, since the cortex is sometimes referred to be a slightly anisotropic conductor (see the discussion section).

A.5 Lead field matrix

Most inverse EEG and MEG source analysis algorithms are based on precomputed forward solutions for a set of anatomically and physiologically meaningful sources, i.e., right-hand sides $(J^y)_{y \in Y}$. It is then advantageous to precompute the so-called *lead field matrix* $L \in \mathbb{R}^{m \times \#Y}$, whose entry $L_{i,y}$ is the forward computed field for source y at sensor i. The lead field matrix can be computed by

(1) multiplying each right-hand side b^y with the transfer matrix T in $\mathcal{O}(mN\#Y)$ and each analytic solution $u^{\infty,y}$ by $\hat{A}$, or

(2) multiplying each row of the transfer matrix T (from the left) by the matrix $B \in \mathbb{R}^{N \times \#Y}$, $B_{i,y} := b_i^y$, of right-hand sides (and adding the term $\hat{A}u^{\infty,y}$). The complexity for the naive approach would again be $\mathcal{O}(mN\#Y)$. However, the matrix B can be cast into the $\mathcal{H}$-matrix format (Wolters et al., 2004) so that each matrix-vector multiplication is of complexity $\mathcal{O}(N \log N)$. The multiplication $\hat{A}u^{\infty,y}$ can as well be per-

formed after casting the right-hand sides $u^{\infty,y}$ into the $\mathcal{H}$-matrix format. Hence, the total complexity reduces in this case to $\mathcal{O}(mN \log N)$. This approach is an ongoing work of the authors that will be published elsewhere.

2 Acknowledgement

This work was supported by the Deutsche Forschungsgemeinschaft (WO1425/1-1, GR3179/1-1, JU 445/5-1). The authors would like to thank J.C. de Munck for providing the software for the quasi-analytical solution in multilayer sphere models and for his quick responses whenever needed.

References

Awada K., Jackson D., Williams J., Wilton D., Baumann S., Papanicolaou A. (1997): Computational aspects of finite element modeling in EEG source localization. IEEE Trans Biomed. Eng. 44(8):736–751.

Baumann S., Wozny D., Kelly S., Meno F. (1997): The electrical conductivity of human cerebrospinal fluid at body temperature. IEEE Trans Biomed. Eng. 44(3):220–223.

Bertrand O., Thévenet M., Perrin F. (1991): 3D finite element method in brain electrical activity studies. In: Nenonen J., Rajala H., Katila T. (Eds.), Biomagnetic Localization and 3D Modelling. Report of the Dep. of Tech.Physics, Helsinki University of Technology pp. 154–171.

Braess D. (2007): Finite Elements: Theory, Fast Solvers and Applications in Solid Mechanics. Cambridge University Press.

Buchner H., Knoll G., Fuchs M., Rienäcker A., Beckmann R., Wagner M., Silny J., Pesch J. (1997): Inverse localization of electric dipole current sources in finite element models of the human head. Electroenc. Clin. Neurophysiol. 102:267–278.

Calvetti D., Hakula H., Pursiainen S., Somersalo E. (2008): Conditionally gaussian hypermodels for cerebral source localization, submitted for publication.

Cook M., Koles Z. (2006): A high-resolution anisotropic finite-volume head model for EEG source analysis. In: Proc. of the 28th Annual Int. Conf. of the IEEE Engineering in Medicine and Biology Society. pp. 4536–4539.

Dahmen W., Reusken A. (2008): Numerik für Ingenieure und Naturwissenschaftler. Springer-Lehrbuch ISBN 978-3-540-76492-2.

de Munck J., Peters M. (1993): A fast method to compute the potential in the multi sphere model. IEEE Trans Biomed. Eng. 40(11):1166–1174.

de Munck J., van Dijk B., Spekreijse H. (1988): Mathematical dipoles are adequate to describe realistic generators of human brain activity. IEEE Trans Biomed. Eng. 35(11):960–966.

Gencer N., Acar C. (2004): Sensitivity of EEG and MEG measurements to tissue conductivity. Phys.Med.Biol. 49:701–717.

Haase G., Kuhn M., Reitzinger S. (2002): Parallel AMG on distributed memory computers. SIAM J. Sci.Comp. 24(2):410–427.

Hackbusch W. (1992): Elliptic Differential Equations. Theory and Numerical Treatment. Springer-Verlag, Berlin.

Hackbusch W. (1994): Iterative solution of large sparse systems of equations. Springer Verlag, Applied Mathematical Sciences 95.

Hallez H., Vanrumste B., Hese P. V., D'Asseler Y., Lemahieu I., de Walle R. V. (2005): A finite difference method with reciprocity used to in-

corporate anisotropy in electroencephalogram dipole source localization. Phys.Med.Biol. 50:3787–3806.

Hämäläinen M., Hari R., R.Ilmoniemi, Knuutila J., O.Lounasmaa (1993): Magnetoencephalography: theory, instrumentation, and applications to non-invasive studies of the working human brain. Rev.Mod.Phys. 65:413–497.

Kybic J., Clerc M., Abboud T., Faugeras O., Keriven R., Papadopoulo T. (2005): A common formalism for the integral formulations of the forward eeg problem. IEEE Trans. Med. Imag. 24(1):12–18.

Marin G., Guerin C., Baillet S., Garnero L., G. M. (1998): Influence of skull anisotropy for the forward and inverse problem in EEG: simulation studies using the FEM on realistic head models. Human Brain Mapping 6:250–269.

Meijs J., Weier O., Peters M., van Oosterom A. (1989): On the numerical accuracy of the boundary element method. IEEE Trans Biomed. Eng. 36:1038–1049.

Michel C., Murray M., G.Lantz, S.Gonzalez, L.Spinelli, de Peralta R. (2004): EEG source imaging. Clin.Neurophysiol. 115:2195–2222 invited review.

Murakami S., Okada Y. (2006): Contributions of principal neocortical neurons to magnetoencephalography and electroencephalography signals. J.Physiol. 575(3):925–936.

Plonsey R., Heppner D. (1967): Considerations on quasi-stationarity in electrophysiological systems. Bull.math.Biophys. 29:657–664.

Plummer C., Harvey A., Cook M. (2008): Eeg source localization in focal epilepsy: Where are we now? Epilepsia 49(2):201–218.

Pursiainen S. (2007): EEG/MEG forward simulation through h- and p-type finite elements. In: Journal of Physics: Conference Series, Proceedings of Applied Inverse Problems (AIP). pp. 1–11.

Pursiainen S. (2008): Computational methods in electromagnetic biomedical

inverse problems. Ph.D. thesis at the Helsinki University of Technology, Faculty of Information and Natural Sciences, Institute of Mathematics.

Ramon C., Schimpf P., Haueisen J., Holmes M., Ishimaru A. (2004): Role of soft bone, CSF and gray matter in EEG simulations. Brain Topography 16(4):245–248.

Rullmann M., Anwander A., Dannhauer M., Warfield S., Duffy F., Wolters C. (2008): EEG source analysis of epileptiform activity using a 1mm anisotropic hexahedra finite element head model. NeuroImage, in press, http://dx.doi.org/10.1016/j.neuroimage.2008.09.009.

Sarvas J. (1987): Basic mathematical and electromagnetic concepts of the biomagnetic inverse problem. Phys.Med.Biol. 32(1):11–22.

Schimpf P., Ramon C., Haueisen J. (2002): Dipole models for the EEG and MEG. IEEE Trans Biomed. Eng. 49(5):409–418.

Shimony J. S., McKinstry R., E.Akbudak, J.A.Aronovitz, A.Z.Snyder, N.F.Lori, T.S.Cull, T.E.Conturo (1999): Quantitative diffusion-tensor anisotropy brain MR imaging: Normative human data and anatomic analysis. Radiology 212:770–784.

Si H. (2004): TetGen, a quality tetrahedral mesh generator and three-dimensional delaunay triangulator, v1.3, user's manual. Tech. Rep. 9 Weierstrass Institute for Applied Analysis and Stochastics.

Si H. (2007): TetView http://tetgen.berlios.de/tetview.html.

Si H. (2008): Adaptive tetrahedral mesh generation by constrained Delaunay refinement. International Journal for Numerical Methods in Engineering 75(7):856–880.

Si H., Gärtner K. (2005): Meshing piecewise linear complexes by constrained Delaunay tetrahedralizations. In: Proc. 14th International Meshing Roundtable. Sandia National Laboratories pp. 147–163.

Stroud A. H. (1971): Approximate calculation of multiple integrals. Prentice-Hall, Inc.

Tanzer O., Järvenpää S., Nenonen J., E.Somersalo (2005): Representation of bioelectric current sources using whitney elements in finite element method. Phys.Med.Biol. 50:3023–3039.

Tuch D., Wedeen V., Dale A., George J., Belliveau J. (2001): Conductivity tensor mapping of the human brain using diffusion tensor MRI. Proc.Natl.Acad.Sci.USA 98(20):11697–11701.

van den Broek S. (1997): Volume conduction effects in EEG and MEG. Ph.D. thesis Proefschrift Universiteit Twente Enschede, The Netherlands.

Wang K., Zhu S., Mueller B., Lim K., Liu Z., He B. (2008): A new method to derive white matter conductivity from diffusion tensor MRI. IEEE Trans Biomed. Eng. 55(10):2481–2486.

Wendel K., Narra N., Hannula M., Kauppinen P., Malmivuo J. (2008): The influence of CSF on EEG sensitivity distributions of multilayered head models. IEEE Trans. Biomed. Eng. 55(4):1454–1456.

Wolters C., Köstler H., Möller C., Härtlein J., Grasedyck L., Hackbusch W. (2007a): Numerical mathematics of the subtraction method for the modeling of a current dipole in EEG source reconstruction using finite element head models. SIAM J. on Scientific Computing 30(1):24–45.

Wolters C., Kuhn M., Anwander A., Reitzinger S. (2002): A parallel algebraic multigrid solver for finite element method based source localization in the human brain. Comp.Vis.Sci. 5(3):165–177.

Wolters C. H., Anwander A., Berti G., Hartmann U. (2007b): Geometry-adapted hexahedral meshes improve accuracy of finite element method based EEG source analysis. IEEE Trans.Biomed.Eng. 54(8):1446–1453.

Wolters C. H., Grasedyck L., Hackbusch W. (2004): Efficient computation of

lead field bases and influence matrix for the FEM-based EEG and MEG inverse problem. Inverse Problems 20(4):1099–1116.

Yan Y., Nunez P., Hart R. (1991): Finite-element model of the human head: Scalp potentials due to dipole sources. Med.Biol.Eng.Comput. 29:475–481.

Zhang Y., Ding L., van Drongelen W., Hecox K., Frim D., He B. (2006): A cortical potential imaging study from simultaneous extra- and intra-cranial electrical recordings by means of the finite element method. NeuroImage 31(4):1513–1524.

Table 1

Quadrature formulas of Stroud (Stroud, 1971) for the volume integral from Equation (12) and the surface integral from Equation (13) .

Formula	degree	number integration points	Reference
Volume integral from Equation (12)			
$T_n : 1-1$	1	1	(Stroud, 1971, Chapter 8.8, p.307)
$T_n : 2-1$	2	$n+1$	(Stroud, 1971, Chapter 8.8, p.307)
$T_3 : 7-1$	7	64	(Stroud, 1971, Chapter 8.8, p.315)
Surface integral from Equation (13)			
$T_n : 1-1$	1	1	(Stroud, 1971, Chapter 8.8, p.307)
$T_n : 2-1$	2	$n+1$	(Stroud, 1971, Chapter 8.8, p.307)
$T_2 : 7-1$	7	16	(Stroud, 1971, Chapter 8.8, p.314)

Table 2

Parameterisation of the anisotropic four layer sphere model.

Medium	Scalp	Skull	CSF	Brain
Outer shell radius	92mm	86mm	80mm	78mm
Tangential conductivity	0.33S/m	0.042S/m	1.79S/m	0.33S/m
Radial conductivity	0.33S/m	0.0042S/m	1.79S/m	0.33S/m

Table 3

The number of nodes and elements of the three tetrahedral models used for numerical accuracy tests.

Model	Nodes	Elements
tet360K	360,056	2,165,281
tet287K	287,217	1,712,360
tet39K	38,928	229,311

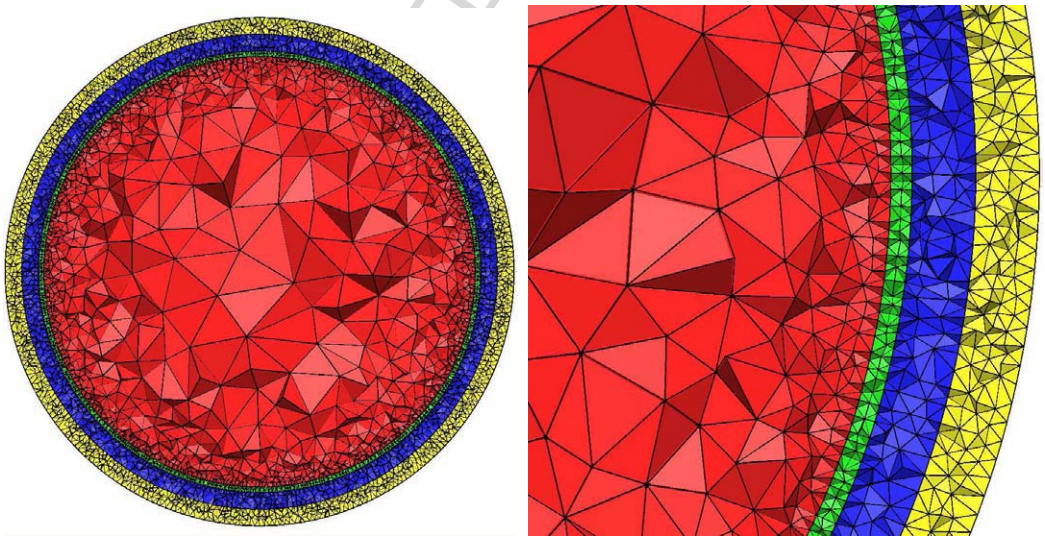

Fig. 1. Cross-section of the tetrahedral mesh `tet360K` of the four compartment sphere model. Visualisation was done using Tetview (Si, 2007).

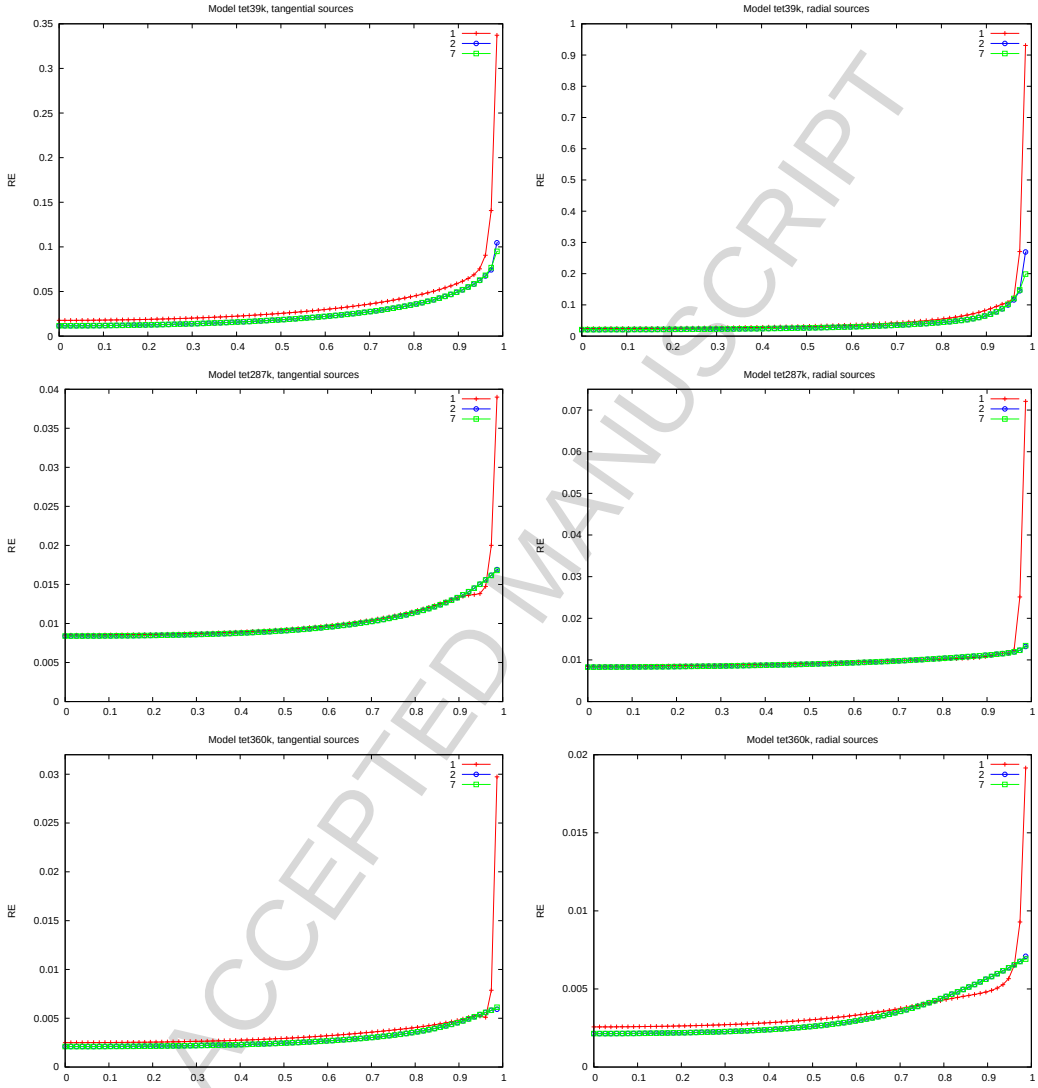

Fig. 2. Relative error for tangentially (left) and radially (right) oriented dipoles with quadrature orders of 1,2 and 7: Model `tet39K` (top row), `tet287K` (middle row) and `tet360K` (bottom row). Note the different scaling for the RE.

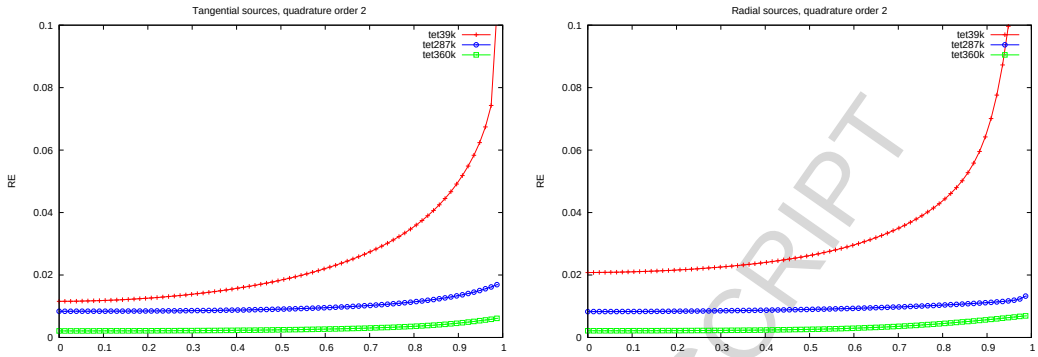

Fig. 3. Relative error for the FE meshes of Table 3 and quadrature order 2 for tangentially (left) and radially oriented dipoles (right).

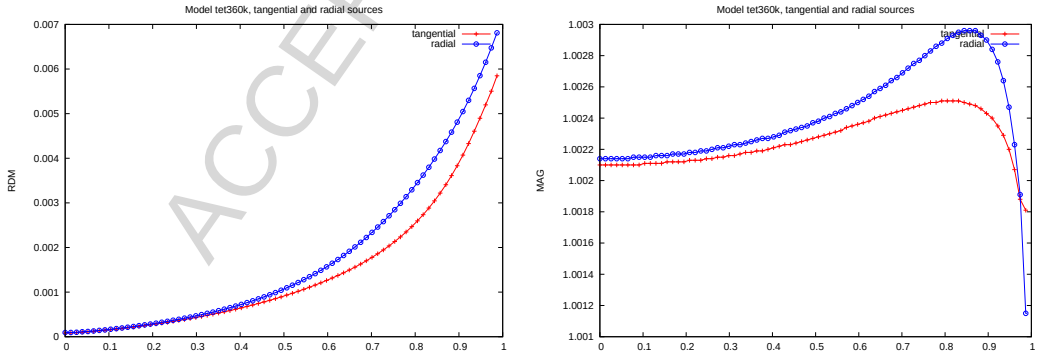

Fig. 4. RDM (left) and MAG errors (right) for model `tet360K` for tangentially and radially oriented dipoles.

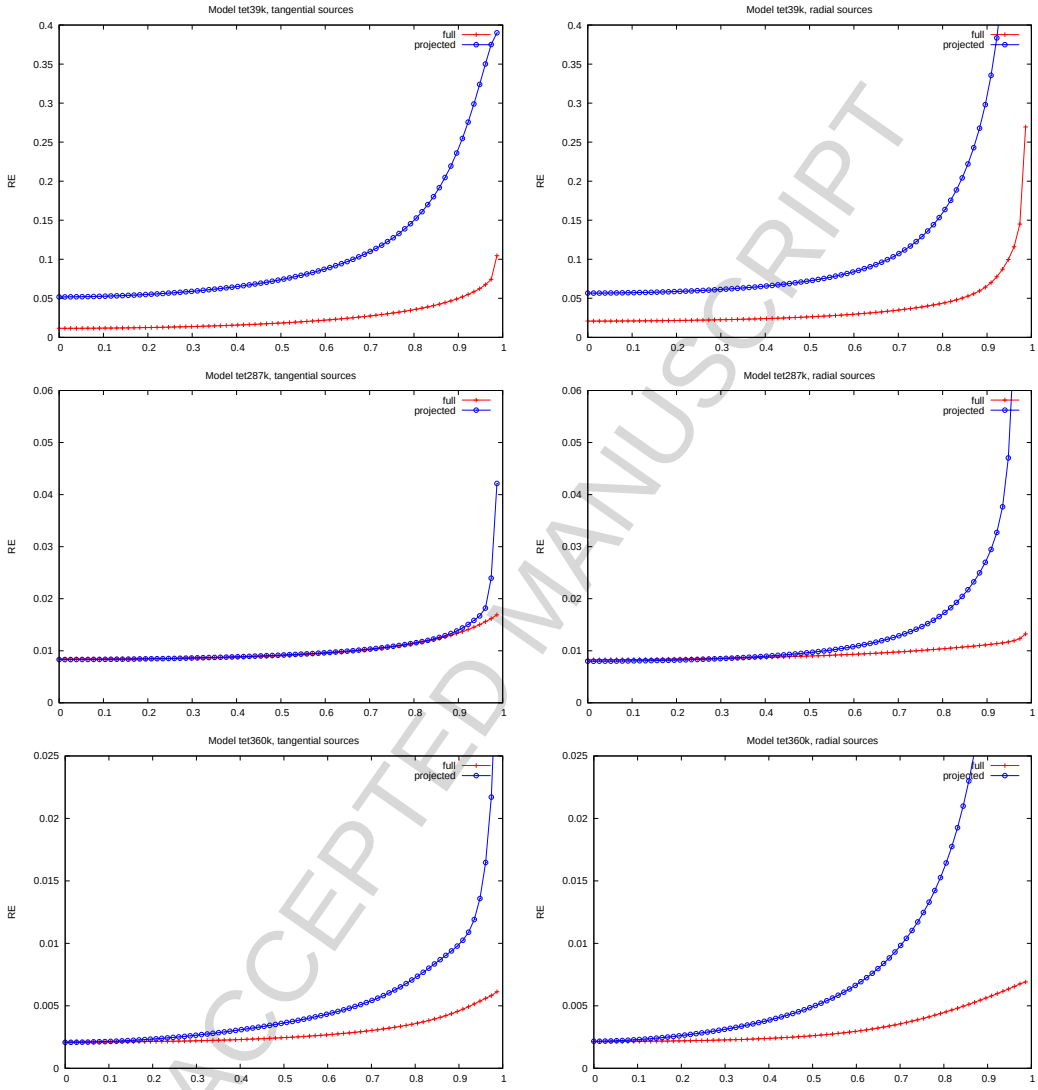

Fig. 5. Comparison between the presented full subtraction approach and the projected subtraction approach from (Wolters et al., 2007a) with regard to the relative error for tangential (left) and radial sources (right): Model `tet39K` (top row), `tet287K` (middle row) and `tet360K` (bottom row).